

Anomalous Ekman Transport Near Kerguelen Island

C. J. Roach¹, H. E. Phillips¹, N. L. Bindoff^{1,2,3,4} and S. R. Rintoul^{2,4}

¹ Institute for Marine and Antarctic Studies, University of Tasmania, Hobart, Tasmania 7001, Australia

² Antarctic Climate and Ecosystems Cooperative Research Centre, Hobart, Tasmania 7001, Australia

³ Tasmanian Partnership for Advanced Computing, Hobart, Tasmania 7001, Australia

⁴ CSIRO Marine & Atmospheric Research, Hobart, Tasmania 7001, Australia

Abstract

In this study we use data from 8 velocity profiling floats to examine the wind driven response of the surface layer of the Southern Ocean north of the Kerguelen Plateau during 2008.

Assuming a constant geostrophic velocity within the upper 200m of the ocean we have identified Ekman-like spirals in 249 profiles and in the mean profile. Considering constant geostrophic shear this figure increased to 455 Ekman spirals.

Mean Ekman transport was found to be skewed towards the wind, lying at 45° rather than 90° to the left of the wind as expected from steady-state Ekman theory for the Southern Hemisphere.

This downwind transport anomaly was found to display little sensitivity to the presence of geostrophic shear or transient wind forcing. We suggest that the anomaly results from the ‘compression’ observed in the mean spiral, possibly associated with ocean density stratification.

Introduction

While the steady state theory behind the interactions between wind stress, the near-surface layers of the ocean and the Coriolis force is well understood [3], field observations are still sparse, particularly in the Southern Ocean. In the classical steady-state case the balance between wind stress and the Coriolis force drives the formation of Ekman spirals which have a characteristic exponential decay of velocity and an anticyclonic (anticlockwise in the Southern Hemisphere) rotation with increasing depth. The net transport arising from Ekman currents is significant to the global meridional overturning circulation, driving the upwelling of deep waters [12] and transporting them northward, and contributing to the formation of Mode Waters [9].

In this paper we present estimates of Ekman transport within the Kerguelen Island region derived from EM-APEX velocity profiling float measurements and present an explanation of an unexpected downwind component of transport. The EM-APEX (Electro-Magnetic Autonomous Profiling eXplorer) is a sophisticated enhancement of the Argo profiling float [11]. It uses motional induction to make high-vertical resolution measurements of horizontal velocity in the ocean, in addition to the standard Argo measurements of temperature and salinity.

Method

Isolating and Diagnosing Ekman Velocities

The eight EM-APEX velocity profiling floats [10] were deployed north of Kerguelen Island in November 2008 in conjunction with the Southern Ocean FINE-structure (SOFINE) expedition. The floats returned over 1600 profiles with samples spaced approximately 3m in the vertical. Horizontal separation of profiles was approx. 2-10 km.

Within the Kerguelen Island region all floats took four profiles (two descent-ascent cycles) per day, spaced to place consecutive pairs of up and down casts approximately half an inertial period (close to 8 hours) apart. This allowed us to isolate the inertial component of velocity [5], which was then removed to leave only the sub-inertial component.

In line with previous studies [2, 4] we assumed there was no geostrophic shear within the mixed layer, allowing both barotropic tides and geostrophic flow to be removed by subtracting a constant reference velocity from the isolated sub-inertial velocity profile. The reference velocity for a given profile was approximated as the mean sub-inertial velocity between 100m and 200m depth on that profile.

The theoretical Ekman spiral can be separated into a velocity amplitude component decaying exponentially with increasing depth and a unit vector component rotating anticlockwise as a linear function of increasing rotation (z , positive upwards):

$$\left| u_{ek}(z) + i v_{ek}(z) \right| = V_{surf} e^{\frac{z}{D_e}} \quad (1a)$$

$$\theta(z) = \frac{z}{D_e} \quad (1b)$$

Where V_{surf} is the surface velocity; D_e is the e-folding depth and $\theta(z)$ is the heading of the Ekman velocity relative to the surface velocity.

Equations 1a and 1b were fitted independently to the upper 50m of each velocity profile using a least squares technique, producing two estimates of decay scale, D_{amp} , the amplitude fit (from 1a) and D_{rot} , the rotational fit (from 1b). The fraction of variance (R^2 value) within the data captured by equations 1a and 1b were calculated for each profile. If the amplitude R^2 exceeded 0.75, the rotational R^2 exceeded 0.5 and a ‘logical’ D_{amp} (less than 500m) was obtained, the profile was classified as

displaying a spiral and the direction of rotation was obtained from the sign of D_{rot} .

Eddy viscosities (k) were then calculated from estimated Ekman layer depths D_{amp} and D_{rot} and the Coriolis parameter (f) as:

$$k = \frac{D_e^2 |f|}{2} \quad (2)$$

Calculating Transport

All profiles were rotated into a wind-relative reference frame using wind estimates interpolated onto each profile's location and time from the CERSAT blended reanalysis-scatterometer wind fields [1], and mapped onto a regular 2m depth grid. This suppresses variability arising from variable wind heading and allows our results to be compared with prior studies [7, 11]. Volume transport per unit path length (T) was obtained for each velocity profile by integrating observed velocities upwards from 200m to the surface-most velocity observation (z_i):

$$T(z) = \int_{200m}^{z_i} (u_e + iv_e) dz \quad (3)$$

The mean wind-relative transport was calculated by averaging all transport estimates. The observed near surface transport was then compared with estimates calculated from reanalysis winds using the well-established relationship [2]:

$$T_x = \frac{\tau_y}{f\rho}, \quad T_y = \frac{-\tau_x}{f\rho} \quad (4)$$

Where τ denotes surface wind-stress and ρ denotes density.

Error bars based on 95% confidence intervals were estimated assuming one degree of freedom per 4 profiles (approximately one degree of freedom per day).

Results

In total, we detected 249 profiles displaying Ekman spirals and another 186 with Ekman-like decay but reverse rotation, possibly consistent with cyclonic super-inertial wind forcing [8]. Ekman spirals were also observed in the mean velocity profiles in both the geographic (not shown) and wind-relative (Figure 1) reference frames.

	Decay Scale (m)	Viscosity ($m^2 s^{-1}$)
Ekman Spirals		
Rotational Fit	43	0.0953
Amplitude Fit	25	0.0322
All Data		
Rotational Fit	93	0.4460
Amplitude Fit	63	0.2047

Table 1. Mean decay scales and eddy viscosities from observations.

Ekman layer depths and resulting eddy viscosities (Table 1) were found to be consistent with previous observations within the Antarctic Circumpolar Current [3, 4]. Estimates of Ekman layer depth from velocity decay were found to be approximately half that estimated from current rotation with depth. This difference in depths indicates a ‘‘compression’’ of the Ekman spiral such that amplitude decays much faster than predicted. ‘Compressed’ spirals have been observed in previous studies [2, 4, 7] which also found a ratio of D_{rot} to D_{amp} close to 1:2, it has been suggested this compression may be linked to stratification within the surface layers of the ocean [6].

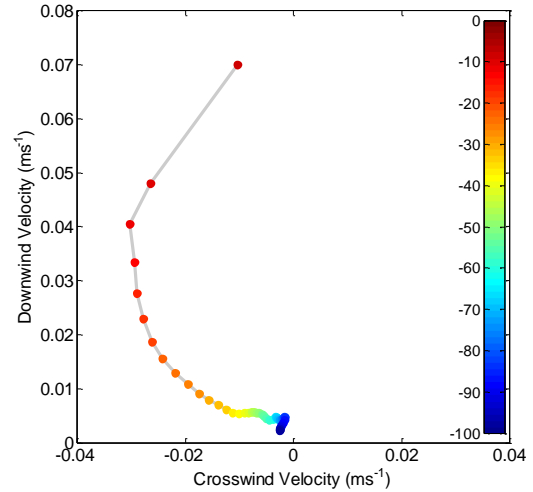


Figure 1. Mean EM-APEX velocity profile, displaying typical behaviour of an Ekman spiral with ocean velocity vectors deflected progressively further to the left of the wind with increasing depth. The colorbar indicates sample depth (metres). The wind direction is up the page.

The mean observed near-surface transport (integrated from 200m to 14m depth) of $0.93 \pm 0.28 m^2 s^{-1}$ was consistent with corresponding wind-based estimates of $1.01 \pm 0.11 m^2 s^{-1}$. Despite this match in magnitude, observed transport heading (Figure 2) did not agree with the theoretical case, sitting at 48° off the wind rather than 90° as expected from steady state Ekman theory.

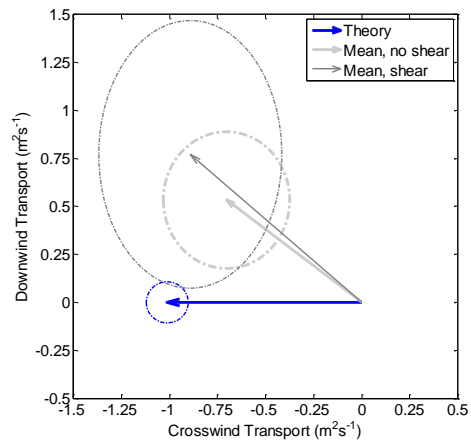


Figure 2: Wind-relative vector plots of mean Ekman transport between 200m and 14m.

This difference in transport heading is not only contrary to ‘classical’ Ekman theory, it is also inconsistent with previous field studies [4]. In the rest of this paper we will

explore potential explanations including the possibility of a subset of the data driving the skewing; conflation of non-uniform geostrophic flow with Ekman currents; the effect of compression of the spirals and the effect of time varying wind forcing.

Partitioning Transport

We divided transport into three distinct subsets based on the structure of the corresponding velocity profiles: Ekman spirals, clockwise turning spirals and non-spiral profiles (Figure 3) to determine whether a specific type of velocity profile was causing the downwind skewing.

Mean transport (T_{tot}) at one depth over all data was considered as the vector sum of mean transport (T_i) over the subsets scaled by the fraction of the dataset a given subset made up (n_i/n):

$$\overline{T}_{tot} = \sum \overline{T}_i \frac{n_i}{n_{tot}} \quad (5)$$

It is apparent that a sizable fraction of the downwind transport was associated with clockwise turning (reverse) spirals, despite these profiles making up only a small fraction of the total dataset. On removing reverse spirals, mean transport heading was found to shift from 48° to 63° left of the wind (Figure 5), improving the agreement with theory, but not to within the 95% confidence level.

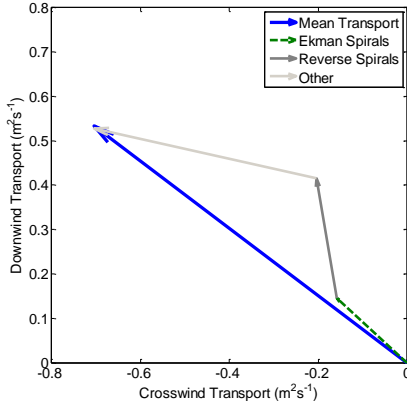


Figure 3. Vector sums of components (transport multiplied by fraction of dataset) for the no shear case (a, top)

Introducing Non-Uniform Geostrophic Flow

In previous studies, and in the results presented above, it has been assumed that geostrophic velocities are constant within the Ekman layer [2, 4]. This assumption is not supported by observations [5]. In our observations the Antarctic Circumpolar Current is a strong depth-varying current aligned with the direction of the wind. It is therefore possible that depth-varying geostrophic flow has been included into our estimate of the Ekman velocity, causing a downwind deflection of the Ekman transport.

We explored the possible effects of non-zero geostrophic shear by assuming that non-inertial currents between 100m and 200m could be described as the sum of a weak Ekman component, a deep reference velocity (here taken as the velocity at the 200m level) and a component arising from a constant geostrophic shear. We used a Nedler-Mead simplex search to optimise the linear shear and Ekman decay scale for each profile. Ekman velocities were then estimated by subtracting the fitted

linear geostrophic velocity profile from the subinertial velocities. Amplitude and rotational fits and classification were then applied as described above.

Inclusion of shear in the velocity field improved the results as indicated by the increased number of Ekman-like spirals (455) and reduction in the number of reversed spirals (109). However, the mean transport was found to display wider confidence intervals and a similar downwind rotation as the no-shear case (Figure 2).

A histogram of transport for each profile revealed that much of this mean downwind transport resulted from a handful of profiles at the far tails of an otherwise Gaussian distribution (not shown). Most of these profiles were associated with strong zonal shear (not shown) likely introduced by the shear fitting procedure.

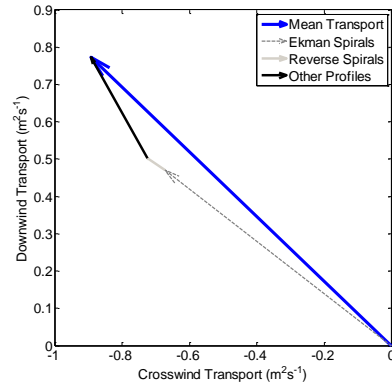


Figure 4. Vector sums of components (transport multiplied by fraction of dataset) for assuming constant non-zero geostrophic shear case.

Figure 4 shows the transport for the subset profiles and all profiles when geostrophic shear in the Ekman layer is accounted for. Transport arising from the Ekman spiral like profiles accounted for 75% of the crosswind transport and 60% of the mean downwind transport. Reverse spirals were found to make only a minor contribution.

A small percentage of the 455 Ekman like spirals, displayed strong zonal shear ($>0.001s^{-1}$, for 18 profiles, $<-0.001s^{-1}$ for 11 profiles), as discussed above. Excluding these profiles had little effect (Figure 5); transport heading remained comparable to the no shear case (47° left of the wind).

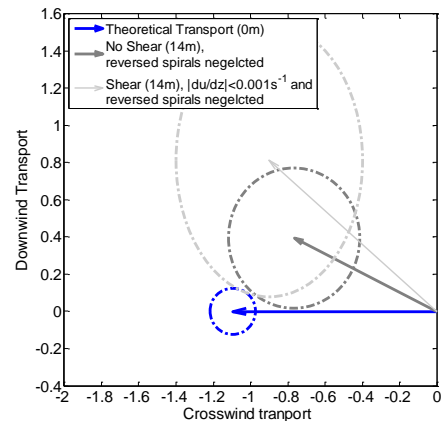


Figure 5. Transport vectors with reversed spirals and Ekman spirals with strong shear removed.

Compressed Spirals and Stratification

To fully examine the effect of a compressed mean spiral on net Ekman transport one would need to consider a complex model explicitly including density stratification. Here we examined the effects of compressed mean spirals in a simplified manner by considering the archetypical Ekman solutions but assuming independent decay scales for rotation (D_{rot}) and amplitude decay (D_{amp}):

$$u_{ek} + iv_{ek} = V_{surf} e^{\frac{z}{D_{amp}}} e^{i(\frac{z}{D_{rot}} + \frac{\pi}{4})} \quad (6)$$

We created synthetic spirals with decay scale ratios (D_{rot} : D_{amp}) between 1:0.25 and 1:5 and calculated the resulting wind relative transport heading between 200m and 14m (Figure 6). Spirals displaying a level of compression comparable to that seen in our observations (between 1:1.5 and 1:3) were found to display transport at the 14m level skewed between 88° and 68° left of the wind, suggesting that ‘‘compression’’ of the mean spiral could account for some of the downwind shift in transport.

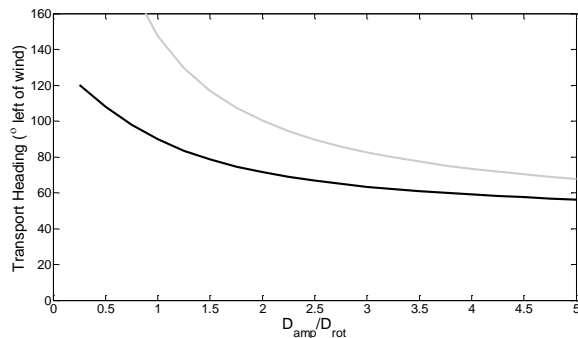


Figure 6: Wind relative heading (black, surface; grey 14m depth) of transport given mean Ekman-like spirals of varying compression.

Time Varying Forcing

To investigate the effects of time varying wind forcing we applied a numerical model of the ‘linear’ Ekman response to a timeseries of winds experienced by one of the floats. While instantaneous transport was frequently different from steady state Ekman theory (not shown), in a time-mean sense it maintained good agreement with the steady state solution and so cannot account for the observed downwind rotation of Ekman transport heading.

Conclusion

We have detected and characterised Ekman spirals using EM-APEX velocity profiling floats in the Southern Ocean. Eddy viscosities were found to range between 322 and $4460 \text{ cm}^2 \text{ s}^{-1}$, in general agreement with previous studies in the Southern Ocean [3, 4]. Ekman spirals were found to be ‘compressed’ with amplitude decaying around twice as fast as the rate of rotation, consistent with prior observations of open-ocean Ekman spirals [4].

Assuming no geostrophic shear within the Ekman layer, mean observed transport was found to be of the same magnitude as expected from wind data and steady state Ekman theory. But, in contravention of theory, Ekman transport heading was skewed downwind.

The downwind transport heading anomaly proved surprisingly robust. Introduction of geostrophic shear within the Ekman layer was found to have little effect on the magnitude and heading of the mean transport but almost doubled the number of spirals detected. Similarly, transient wind forcing was not able to account for the skewing of heading. There is some indication that compression of the mean Ekman spiral, likely associated with stratification, may explain the transport anomaly.

Further investigation of the observed transport heading anomaly is necessary including a more realistic examination of the role of stratification and an examination of the effects of surface waves on the velocity profiles.

References

- [1] *Blended Wind Fields - User Manual*. 2006, Centre ERS d’Archivage et de Traitement.
- [2] Chereskin, T.K., *Direct evidence for an Ekman balance in the California Current*. Journal Of Geophysical Research, 1995. **100**: p. 18261-18269.
- [3] Elipot, S. and S.T. Gille, *Ekman layers in the Southern Ocean: spectral models and observations, vertical viscosity and boundary layer depth*. Ocean Science, 2009. **5**(2): p. 115-139.
- [4] Lenn, Y. and T.K. Chereskin, *Observation of Ekman Currents in the Southern Ocean*. Journal Of Physical Oceanography, 2009. **39**: p. 768-779.
- [5] Phillips, H.E. and N.L. Bindoff, *Observations of non-‘‘equivalent barotropic’’ flow in the Antarctic Circumpolar Current*. In preparation for Journal Of Geophysical Research.
- [6] Price, J.F. and M.A. Sundermeyer, *Stratified Ekman Layers*. Journal Of Geophysical Research, 1999. **104**(C9): p. 20467-20494.
- [7] Price, J.F., R.A. Weller, and R.R. Schudlich, *Wind-Driven Ocean Currents and Ekman Transport*. Science, 1987. **238**: p. 1534-1538.
- [8] Rudnick, D.L. and R.A. Weller, *Observations of Superinertial and Near-Inertial Wind-driven Flow*. Journal Of Physical Oceanography, 1993. **23**: p. 2351-2359.
- [9] Sallée, J.-B., et al., *Formation of subantarctic mode water in the southeastern Indian Ocean*. Ocean Dynamics, 2006. **56**: p. 525-542.
- [10] Sanford, T.B., et al., *Autonomous velocity and density profiler: EM-APEX*, in *IEEE/OES Eighth Working Conference on Current Measurement Technology*. 2005, IEEE: University of Southampton. p. 152-156.
- [11] Schudlich, R.R. and J.F. Price, *Observations of Seasonal Variation in the Ekman Layer*. Journal Of Physical Oceanography, 1998. **28**: p. 1187-1204.
- [12] Speer, K., S.R. Rintoul, and B. Sloyan, *The Diabatic Deacon Cell*. Journal Of Physical Oceanography, 2000. **30**: p. 3212-3222.